Detecting Tree-like Multicellular Life on Extrasolar Planets

Christopher E. Doughty and Adam Wolf

Abstract

Over the next two decades, NASA and ESA are planning a series of space-based observatories to find Earth-like planets and determine whether life exists on these planets. Previous studies have assessed the likelihood of detecting life through signs of biogenic gases in the atmosphere or a red edge. Biogenic gases and the red edge could be signs of either single-celled or multicellular life. In this study, we propose a technique with which to determine whether tree-like multicellular life exists on extrasolar planets. For multicellular photosynthetic organisms on Earth, competition for light and the need to transport water and nutrients has led to a tree-like body plan characterized by hierarchical branching networks. This design results in a distinct bidirectional reflectance distribution function (BRDF) that causes differing reflectance at different sun/view geometries. BRDF arises from the changing visibility of the shadows cast by objects, and the presence of tree-like structures is clearly distinguishable from flat ground with the same reflectance spectrum. We examined whether the BRDF could detect the existence of tree-like structures on an extrasolar planet by using changes in planetary albedo as a planet orbits its star. We used a semi-empirical BRDF model to simulate vegetation reflectance at different planetary phase angles and both simulated and real cloud cover to calculate disk and rotation-averaged planetary albedo for a vegetated and non-vegetated planet with abundant liquid water. We found that even if the entire planetary albedo were rendered to a single pixel, the rate of increase of albedo as a planet approaches full illumination would be comparatively greater on a vegetated planet than on a non-vegetated planet. Depending on how accurately planetary cloud cover can be resolved and the capabilities of the coronagraph to resolve exoplanets, this technique could theoretically detect tree-like multicellular life on exoplanets in 50 stellar systems. Key Words: TPF—Darwin—Extrasolar planets—Astrobiology—BRDF—Remote sensing—multicellular life. Astrobiology 10, 869–879.

1. Introduction

OVER THE NEXT FEW DECADES, NASA and ESA are planning a series of space-based observatories to measure the spectra from Earth-sized extrasolar planets in regions where liquid water may be present (Lawson *et al.,* 2007; Cockell *et al.,* 2009). There has been much justifiable interest in developing methods of detecting life on these planets. Planetary biosignatures that have been considered include biogenic gases in the atmosphere (O_2 in the presence of H_2O, O_3, CH_4 with O_2, CH_3Cl, N_2O) (Des Marais *et al.,* 2002) and surface reflectance spectra of vegetation (Ford *et al.,* 2001; Seager *et al.,* 2005; Tinetti *et al.,* 2006a, 2006b; Kiang *et al.,* 2007a, 2007b).

A potential biosignature is a planet's absorption spectrum (Kiang *et al.,* 2007b). Earth's plants have a sharp, order-of-magnitude increase in leaf reflectance between 700 and 750 nm wavelengths due to the difference between photosynthetic absorption of photons (between 400 and 700 nm) and reflectance and scattering at higher wavelengths not used for photosynthesis (>700 nm). Seven hundred nanometers is in the red part of the electromagnetic spectrum, and the reflectance contrast is referred to as the "red edge". Such a sharp, order-of-magnitude change in reflectance is rare in nature, and Earth's red edge has been confirmed as a planetary biosignature both in the spectrum of Earthshine (spatially integrated light scattered off the Moon and reflected to Earth) (Seager *et al.,* 2005; Palle *et al.,* 2009) and by remote sensing from the Galileo spacecraft (Sagan *et al.,* 1993). Researchers have theorized that water-splitting photosynthesis is the only type of photosynthesis efficient enough to support plentiful life on an extrasolar planet (Wolstencroft and Raven, 2002). The wavelength of an edge-like reflectance feature like the red edge could theoretically be determined if the planet's distance from the Sun and the photons required to split water at this distance are known (Wolstencroft and Raven, 2002; Kiang *et al.,* 2007b).

If future space observatories such as Terrestrial Planet Finder (TPF; NASA) or Darwin (ESA) succeed in finding a

Department of Global Ecology, Carnegie Institution, Stanford, California.

planet with both biogenic gasses in the atmosphere and a red-edge characteristic of life, we would want to know whether the land-based life on this planet is similar to the green photosynthetic slime common for most of Earth's history (Beerling, 2007) or whether this life has evolved to be diverse and multicellular. For instance, on Earth, the first fossil evidence of land plants, similar to modern bryophytes, was in the Mid-Ordovician (490–430 million years ago) (Graham *et al.*, 2000). Single-celled photosynthetic organisms evolved as early as 3 billion years ago and were present on land as early as 1.2 billion years ago (Horodyski and Knauth, 1994). High $\delta^{13}C$ values in Precambrian rocks indicate that there was a significant cover of single-celled photosynthetic organisms on land during this period (Kenny and Knauth, 2001). Therefore, viewed from space, from 1.2 billion years ago to 490 million years ago, the Earth could have had a red-edge signal and biogenic gases in the atmosphere but no visible multicellular life. Below, we explore the question of whether multicellular life is detectable and whether vegetated planets can be distinguished from planets with less-complex life.

Multicellular life on Earth is characterized by hierarchical branching networks, a topological structure ubiquitous in biology (Brown and West, 2000). For multicellular photosynthetic organisms, this branching network is characterized by a "tree," whose structural attributes and fractal topology are conserved over different phyletic groups and are independent of the environmental conditions that accompany ontogeny (West *et al.*, 1999). Competition for light and the need to transport water and nutrients in multicellular photosynthetic organisms has led to the tree-like structure on Earth that emerges from a few general principles that are widespread in

nature (West *et al.*, 1999). As a consequence of these biomechanical and evolutionary constraints, the tree growth habit has evolved independently several times on Earth (Donoghue, 2005). We make the assumption that such biomechanical constraints combined with Darwinian evolution will likewise produce tree-like structures for photosynthetic multicellular organisms, if they exist, on extrasolar planets.

The same constraints that result in tree-like shapes of individual organisms result in predictable relationships between size, shape, and population density at the stand-level in forests (Enquist *et al.*, 1998; West *et al.*, 2009). These variations in the size and shapes of trees in forest stands result in strong differences in the reflectance of forest canopies as seen from different angles overhead (Li and Strahler, 1992; Bréon *et al.*, 1997, 2002; Wolf *et al.*, 2010).

The bidirectional reflectance distribution function (BRDF) is the change in observed reflectance with changing view angle or illumination direction (Schaepman-Strub *et al.*, 2006). The BRDF is the ratio of the differential radiance (dL) (W m^{-2} sr^{-1}) to the differential irradiance (dE) (W m^{-2}), $f_r(\Omega_I, \Omega_v) = dL(\Omega_I, \Omega_v)/dE(\Omega_I)$, where Ω_i is illumination direction and Ω_v is the viewing direction. Surface albedo results if the BRDF is integrated over the entire viewing hemisphere.

Vegetation indices emerge from the differences in reflectance at the red edge. However, BRDF emerges from geometric optics, that is, the shape and arrangement of objects within a pixel that transmit or block light (Torrance and Sparrow, 1967). When viewed from space, forests appear brighter as the view angle approaches the Sun angle and brightest when the observer is in line with the Sun, a position referred to as the hot spot (Fig. 1). This occurs because at zero
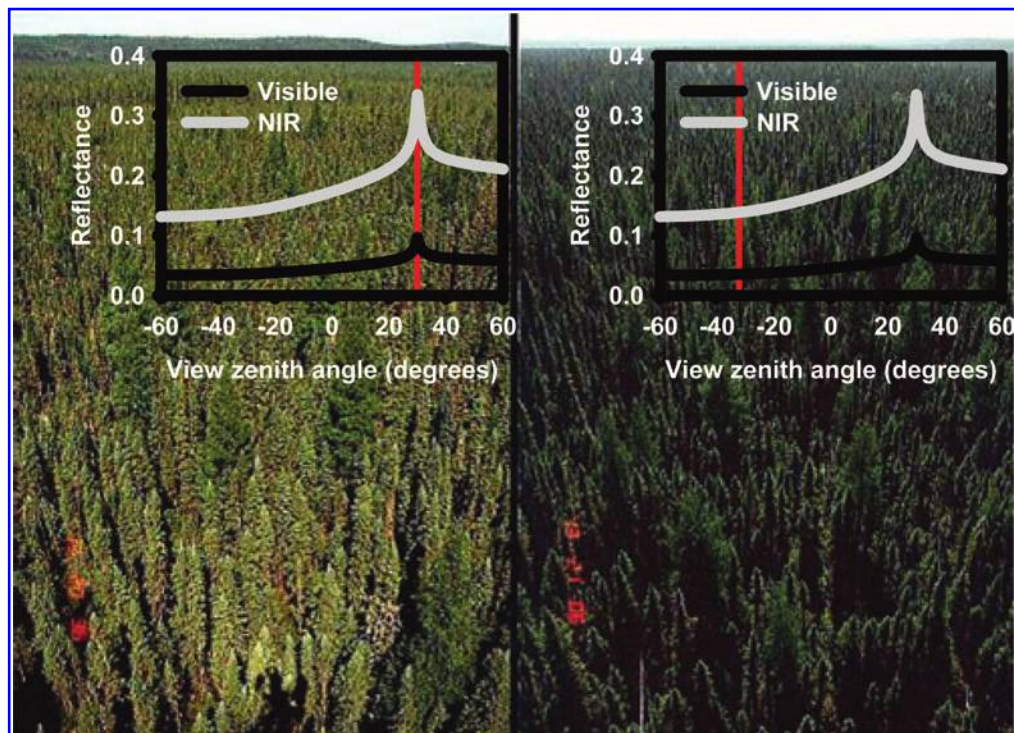

FIG. 1. Canadian black spruce showing backscattering (sun behind observer) on the left and forward scattering (sun opposite observer) on the right. Note the bright region (hot spot) where all shadows are hidden on the left. The graphs show the classic drop-off of BRDF from the hot spot to the dark spot along the principle plane for needle-leaf forest. The red line shows the view zenith angle from each photo. Photograph by Don Deering.

phase angle, all shadows cast by objects are obscured (Hapke *et al.*, 1996), and at higher phase angles more shadows become visible to the observer, which results in a darkening of the pixel's reflectance. The rate of change of the reflectance with phase angle, in both the zenith and azimuth directions, is closely linked to the size, shape, and number of trees in the scene; and there is a quantitative theory of the shape of the BRDF (Li and Strahler, 1992). Observations of the BRDF from space demonstrate that less-structured scenes, such as deserts and tundra, have a flatter BRDF as a function of view zenith angle, and more-structured scenes such as savanna and forest have a more peaked BRDF (Bréon *et al.*, 1997; Bicheron and Leroy, 2000). In this study, we examine whether this technique could be used to detect the existence of tree-like structures on the surface of an extrasolar planet. As far as we are aware, this is the first study to examine the BRDF integrated over the entire planetary disk.

Spectral information from a Darwin- or TPF-type mission will be averaged over the entire disk, because the large distances to the planet prohibit greater spatial resolution, and averaged over a full rotation period, because spectral and temporal sampling will be limited by the relatively low brightness of the planet compared with its parent star. In this study, we developed a method to determine whether multicellular life, specifically canopy structure, could be detected on an Earth-like planet based on spectra that are averaged over the full disk for a full rotation period. We hypothesize that, as Earth approaches full illumination, an observer in line with the star and planet will observe an anomalous increase in albedo as shadows cast by vegetation are blocked by the vegetation (Fig. 2). Without vegetation there would be no anomalous increase in albedo as a planet approaches full illumination. We tested our theory by combining a well-tested BRDF model with a global vegetation map and global cloud data and simulations to model Earth's albedo as viewed by a distant observer between phase angles of $0.5°$ and $44°$.

2. Methods

To calculate disk and rotationally averaged planetary reflectance on a vegetated and non vegetated planet, we first modeled the reflectance for each grid cell at different geometries and phase angles (the angle between the star, the observer, and the planet), using the following semi-empirical model (Maignan *et al.*, 2004; Bacour and Bréon, 2005), based on data from the POLDER instrument (Bicheron and Leroy, 2000):

$$R(\Omega_i, \Omega_v, \varnothing) = k_0 + k_1 F_1(\Omega_i, \Omega_v, \varnothing) + k_2 F_2(\Omega_i, \Omega_v, \varnothing)$$

This equation calculates reflectance (R) for each vegetation type based on its geometry [solar zenith (Ω_i), view zenith (Ω_v), and relative azimuth ($\varnothing$) angles] between phase angles of $0.5°$ and $44°$. It combines a geometric kernel (F_1), which models a flat Lambertian surface covered with randomly distributed spheroids with the same optical properties as soil (Lucht *et al.*, 2000), with a volumetric kernel (F_2), which models a theoretical turbid vegetation canopy with high leaf density (Maignan *et al.*, 2004). The model fixes the hot spot half-width parameter to $1.5°$, the mean observed value (Bréon *et al.*, 2002). K (k_0, k_1, k_2) are biome-dependant constants inverted from multi-angle reflectance data collected in the global POLDER satellite database (Bacour and Bréon, 2005). We calculated the reflectance for the visible (670 nm) and the near infrared (NIR) (865 nm) wavelengths. The choice of optimal wavelengths for this method is complicated and is explained in the discussion.

We calculated globally integrated planetary reflectance by combining a global vegetation map ($2°$ by $2.5°$ resolution at the equator) (Oleson and Bonan, 2000) with surface reflectance values calculated for four plant functional types per pixel. The plant functional types used in the model are as follows: evergreen needle leaf forest, evergreen broadleaf forest, deciduous needle leaf forest, deciduous broadleaf forest, mixed forests, closed shrublands, open shrublands, woody savannas, savannas, grasslands, and croplands. Plant functional types distinguish growth form and hence BRDF properties. BRDFs for Earth could also be generated by using the MODIS global BRDF database; however, our method enables manipulation of the land surface.

Abundant multicellular life is more likely to arise on planets with liquid water, an oxygen atmosphere, and active geology (Kasting and Catling, 2003); and these will erode most steep geological features such as asteroid craters or most very steep mountains (>$45°$ tilt). More than 99% of Earth's surface has a slope less than $45°$ (Hall *et al.*, 2005). We removed observations made at high phase angles (45–90°) to
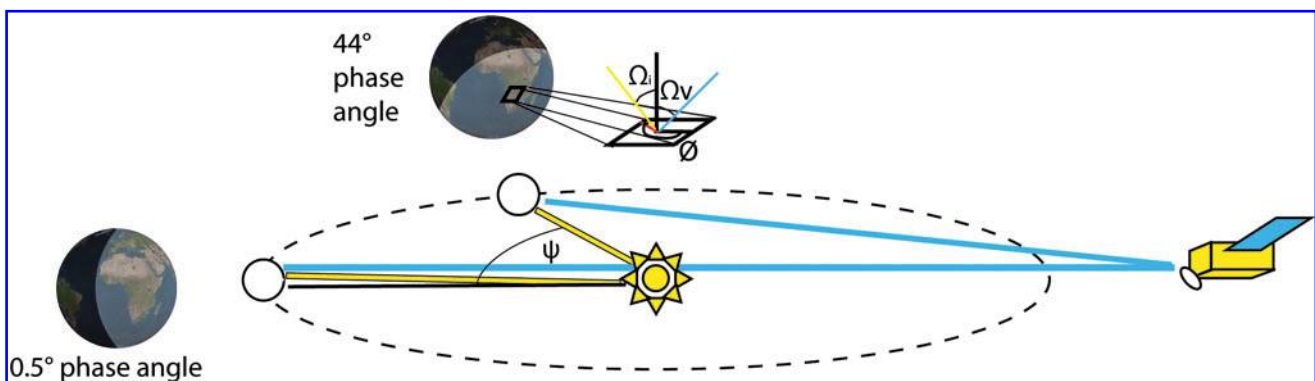

FIG. 2. A diagram of our proposed experimental design. The distant observer, a space telescope such as TPF, would observe the rate of change of albedo near the phase angles of $0.5°$ and $44°$. $\varnothing$ is the azimuth angle, Ω_i is the solar zenith angle, Ω_v is the view angle, and Ψ is the phase angle.

ensure any confounding effect from steep terrain is small. We also did not analyze phase angles between 45° and 90° to avoid forward scattering effects from water and clouds. There are only minor BRDF effects between phase angles of <45° for oceans (Jin *et al.*, 2004), ice, and bare ground (Bicheron and Leroy, 2000). Sensitivity studies indicate that our results are still valid even if reflectance of oceans, ice, and bare ground increases by up to 0.06 at full illumination from backscattering BRDF effects.

We calculated planetary albedo as the integrated disk- and rotation-averaged emitted radiation over 144 simulations representing solar zenith 0° at the equator for each of the 144 longitudinal bands, each with separate view zenith, solar zenith, and azimuth angle for each pixel. In Fig. 3, we show view zenith, solar zenith, and azimuth angles for two such simulations, at 0.5° and 44° phase angles and their resulting reflectance. We assumed no tilt to the planet and further assumed that the observer is in an approximate plane with the planet's orbit and its star. This assumption will be valid for Earth-sized planets detected by the Kepler observatory because it detects planets by using slight changes in the star's brightness as a planet transits. The BRDF technique would require additional geometric calculations for planets that do not meet this assumption. By the cosine effect, pixels near the poles have proportionally less weighting. We used the fol-

lowing formula to calculate the area (A) of each grid cell on our maps:

$$A = \int_{\varphi_1}^{\varphi_2} R \left(\int_{\lambda_1}^{\lambda_2} R^* \cos \varphi \, d\lambda \right) d\varphi = R^2 (\lambda_2 - \lambda_1)(\sin \varphi_2 - \sin \varphi_1)$$

where longitudes are represented by λ_1 and λ_2, latitudes are represented by φ_1 and φ_2, with $0 \le \lambda_1 \le \lambda \le \lambda_2 \le 2\pi$ and $-\pi/2 \le \varphi_1 \le \varphi \le \varphi_2 \le \pi/2$. R is the Earth's radius, and λ_1 and λ_2 are expressed in radians.

Reflected photon flux density of a planet will increase from dichotomy to full illumination as reflected light from a larger portion of the planet reaches the observer. Photons reaching the observer are a function of planetary albedo and the portion of the planet illuminated at different phase angles. In this paper, we define albedo as reflected photons divided by top of atmosphere incident radiation at full illumination.

We simulated global cloud cover using the National Center for Atmospheric Research Community Atmosphere Model (CAM 3.0; http://www.ccsm.ucar.edu/models/atm-cam) (Collins *et al.*, 2006), coupled with the Community Land Model (CLM 3.0; http://www.cgd.ucar.edu/tss/clm) and a slab ocean model. The simulations were run for 60 years at a 20-minute time step and a resolution of 2° by
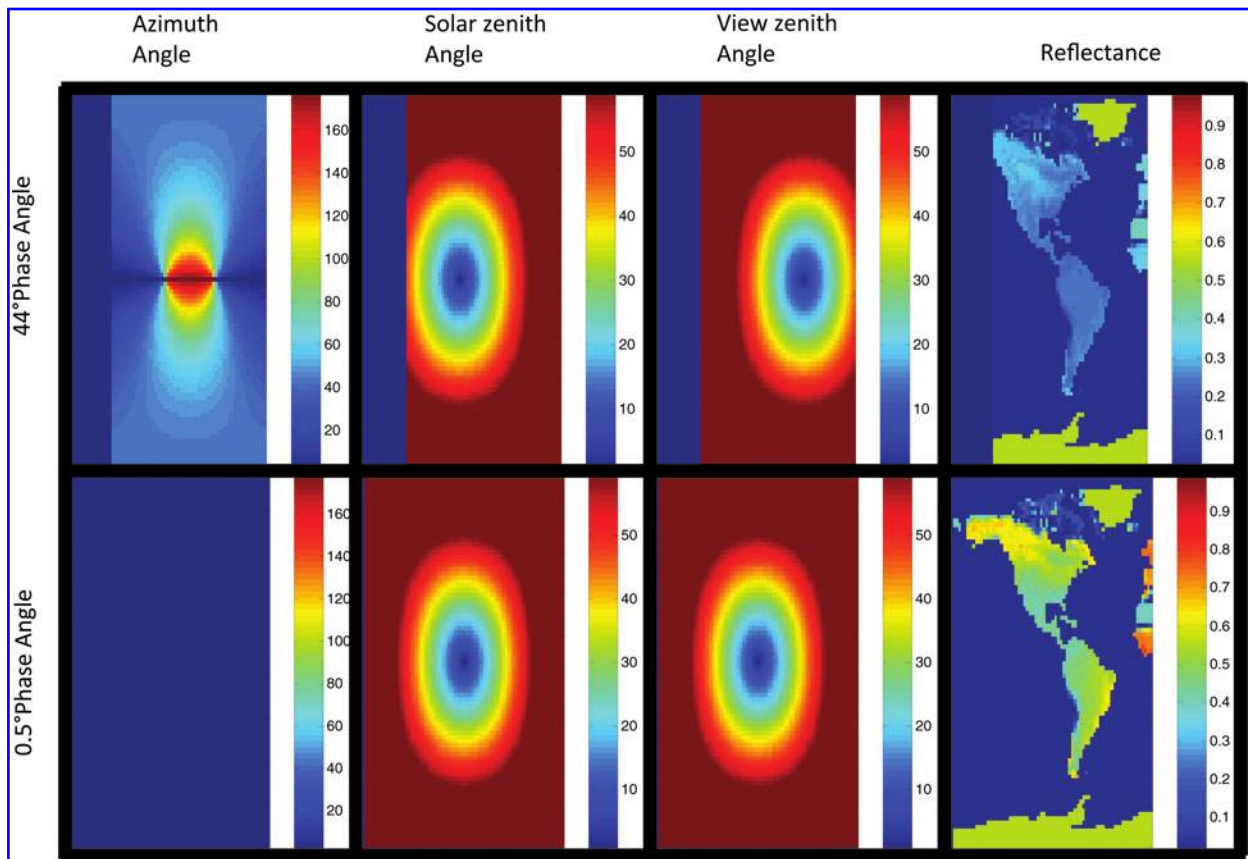

FIG. 3. (From left to right) Azimuth angle, solar zenith angle, view zenith angle used to calculate reflectance (right) at a phase angle of 44° (top) and 0.5° (bottom). The *x* axis is longitude, and the *y* axis is latitude. We averaged 144 such simulations together, one at each longitudinal band, to simulate accurate geometry as a planet rotates for each phase angle. At 0.5° phase angle, the planet is close to 50% illuminated; and at 44° phase angle, the planet is only ∼35% illuminated at any time, which is why the longitudinal bands are larger at 0.5° phase angle than at 44° phase angle.

2.5° at the equator. We simulated cloud cover for a vegetated Earth and a bare-ground Earth to see how vegetation can affect total planetary cloud cover. We combined simulated cloud height (low, medium, and high) and total percent cover with albedo values for low, medium, and high clouds (strato-cumulous, alto-stratus, and cirrus) at several planetary phase angles (Tinetti *et al.,* 2006a). To calculate accurate monthly and annual cloud variability on Earth, we used 10 years (1986–1995) of an observational cloud data set, International Satellite Cloud Climatology.

Digitized data from Fig. 7 of Tinetti *et al.* (2006b) was used to obtain albedo for clouds (strato-cumulous, alto-stratus, and cirrus) at different planetary phase angles. Descriptions of the physics of this planetary model and further information on the data sets are available in papers by Tinetti *et al.* (2006a) and Tinetti *et al.* (2005). Albedo for each pixel was an area-weighted average of land surface albedo calculated by using our BRDF model multiplied by the percentage of the pixel not cloud covered and the albedo of low, medium, and high clouds based on height ratios and percentage cloud cover.

To test whether we could use this method to detect multicellular life under conditions of unknown planetary cloud cover, we varied the total planetary cloud cover between 50% and 70%. To understand how month-to-month changes in global cloud cover may impact albedo, we simulated albedo for each month separately at 50%, 60%, and 70% total planetary cloud cover. We then calculated the difference in the rate of change of albedo between phase angles 0.5° and 3.5° and phase angles 44° and 47° for all 36 simulations.

We tested our method based on two actual coronagraph designs (Guyon *et al.,* 2006). The Achromatic Interferometric Coronagraph (Gay and Rabbia, 1996) has a 50% useful throughput (total amount of planet light, divided by the flux in planet light that is collected by the entrance aperture) at $0.5 \, \lambda \, \mathrm{d}^{-1}$ (Guyon *et al.,* 2006), which is close to the theoretical detection limit. λ is the wavelength of light; d is diameter of the aperture (m). This gives the minimum separation that can be detected between the star and the planet in radians, or the smallest inner working angle. If stellar angular size is considered, the best current coronagraph is the Phase Induced Amplitude Apodization Coronagraph (Guyon *et al.,* 2005), which can detect planets up to $2 \, \lambda \, \mathrm{d}^{-1}$. We calculated how close to its star we could detect an exoplanet based on the two coronagraph designs, a 12 m lens, 400 and 800 nm wavelengths, an Earth-like planetary radius of 1 AU, and varied distance to the star.

3. Results

A cloud-free planet with Earth-like vegetation increases its disk and rotationally averaged integrated albedo from 0.09 in the NIR (865 nm) and 0.06 in the visible (670 nm) at 44° phase angle to 0.18 in the NIR and 0.11 in the visible at 0.5° phase angle. With no vegetation, albedo increases from 0.12 in the NIR and 0.08 in the visible at a phase angle of 44° to 0.15 in the NIR and 0.11 in the visible at 0.5° phase angle. With cloud cover, the vegetated planet's albedo increases from 0.17 in the NIR and 0.14 in the visible at 44° phase angle to 0.53 in the NIR and 0.38 in the visible at 0.5° phase angle (Fig. 4). Without vegetation, a cloudy planet's albedo increases from 0.18 in the NIR and 0.15 in the visible at 44° phase angle to 0.52 in the NIR and 0.38 in the visible at 0.5° phase angle. NIR albedo increases by 0.36 in the NIR and 0.24 in the visible between 0.5° and 44° on a vegetated planet with clouds and by 0.34 in the NIR and 0.23 in the visible on a non-vegetated planet with clouds, a difference of 0.02 and 0.01 (Table 1).

On Earth, clouds dominate planetary albedo, and large variations in cloud cover at different phase angles can cause an increase in brightness that mimics the BRDF effect of vegetation. Over a 10-year period, the yearly averaged International Satellite Cloud Climatology cloud cover averaged 0.64 ± 0.009. Planetary cloud cover can vary by ± 0.011 between the monthly maximum and the monthly minimum with a standard deviation of <1% (0.008) for all months. There were large regional differences between climate simulations for a vegetated planet and a non-vegetated planet, but month to month globally averaged planetary cloud cover only differed by 0.003 on average.
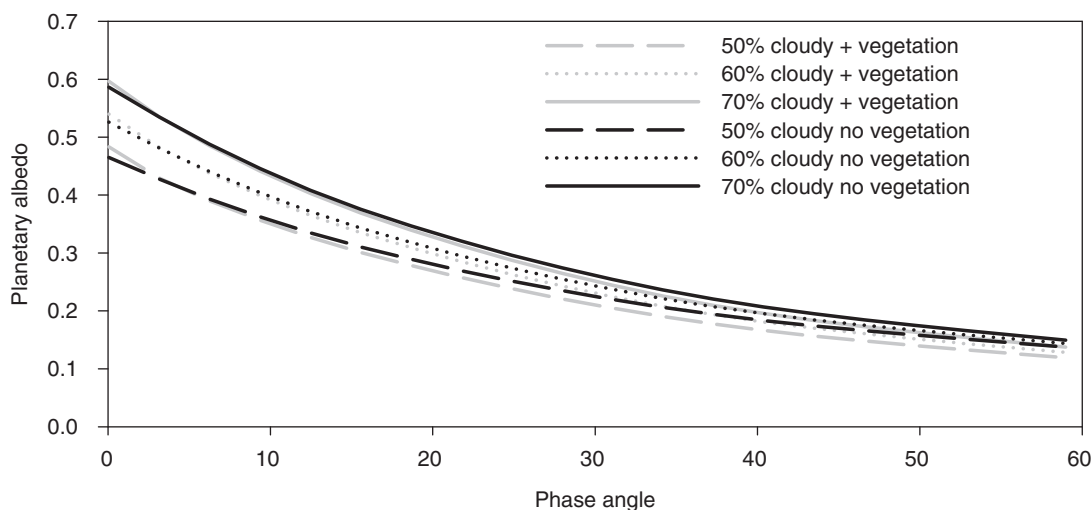

FIG. 4. Planetary albedo at different phase angles at 865 nm for planets with 50% (dashed line), 60% (dotted line), 70% (solid line) cloud cover for a vegetated (gray) and non-vegetated (black) planet.

Table 1. The Increase in Albedo between Phase Angles 0.5° and 44° for a Simulated Planet with No Vegetation, Vegetation, Cloud Cover, and No Cloud Cover

	No vegetation	Vegetation	No vegetation + clouds ± sd	Vegetation + clouds ± sd
Change in visible albedo	0.027	0.043	0.23 ± 0.007	0.24 ± 0.007
Change in NIR albedo	0.037	0.096	0.34 ± 0.012	0.36 ± 0.011

Cloud cover is the average planetary cloud cover for each of the 12 months ($N = 12$). sd, standard deviation.

Increasing cloud cover from 50% to 70% can increase albedo by ∼0.12 at 0.5° but only ∼0.02 at 44° phase angle (Fig. 4). Therefore, a planet with multicellular life cannot be distinguished by subtracting the albedo at phase angle 0.5° from albedo at phase angle 44° because this value will vary depending on total percentage cloud cover, which may not be known with accuracy.

Although an obstacle, it is possible to solve this by exploiting the differing rate of change of planetary albedo because the rate of increase of albedo is much greater between 0.5° and 3.5° than between 44° and 47° on a vegetated planet than on a non-vegetated planet (Fig. 5). Because of this differing rate of change, over a wide range of cloud covers, we were able to distinguish a vegetated planet from a non-vegetated planet, using the second derivative with respect to phase angle of planetary albedo as a planet rotates around its star (Fig. 6). We estimate that the rate of increase in brightness between 0.5° and 3.5° and 44° and 47° can distinguish multicellular life if planetary cloud cover is resolved to ±0.1 in the NIR and ±0.05 in the visible wavelengths (Fig. 6).

We used two coronagraph designs (2 and 0.5 λ d^{-1}) at 400 nm (representing the visible spectrum) and 800 nm (representing the NIR spectrum) to estimate how close to its star a planet's albedo can be measured. We estimate that a coronagraph 2 λ d^{-1} can measure a planet up to 2 light-years away within 1° of its star (Fig. 7). A coronagraph capable of 0.5 λ d^{-1} can measure a planet within 0.5° of its star up to 8 light-years away. At 800 nm, a coronagraph 0.5 λ d^{-1} can measure a planet within 0.5° of its star up to 4 light-years away, and a 2 λ d^{-1} coronagraph could measure up to 1 light-year away.

Based on estimates of how close to its star a planet can be resolved and how well a planet with multicellular life can be distinguished under different levels of planetary cloud cover, we estimate the theoretical maximum distance this technique could potentially be used to detect multicellular life. Using the rate of increase in brightness between 0.5° and 3.5° and 44° and 47° in the NIR, multicellular life may be detected if planetary cloud cover is known within ±0.1 (Fig. 6). A coronagraph 0.5 λ d^{-1} can detect an exoplanet within 0.5° of its star at 2 light-years (Fig. 7). Therefore, a 0.5 λ d^{-1} coronagraph at 800 nm wavelengths can potentially detect multicellular life only to 2 light-years if planetary cloud cover can be resolved to ±0.1 accuracy (Fig. 8). The optimal wavelength is 800 nm unless cloud cover can be resolved to better than ±0.03; then 400 nm is the optimal wavelength (Fig. 8). We assume that it will be difficult to resolve planetary cloud cover to better than ±0.02 and do not show this section of the graph because on Earth month-to-month cloud cover can vary by ±0.01.

4. Discussion

A planet with multicellular life would have a peak in brightness as it approaches full illumination due to anisotropic effects that would not be present on a lifeless planet
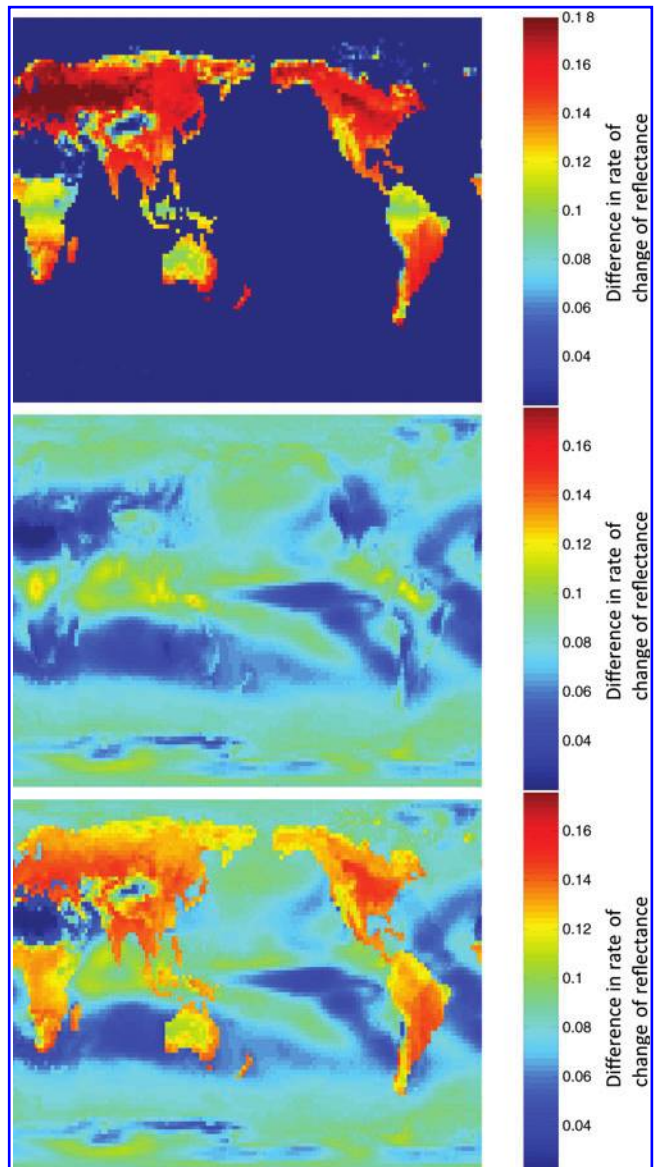

FIG. 5. The difference in the rate of change of albedo at 865 nm between phase angles 0.5° and 3.5° and 44° and 47° for a vegetated planet with no clouds (top), a cloudy planet with no vegetation (middle), and a cloudy planet with vegetation (bottom).

FIG. 6. Change in the rate of increase of integrated planetary albedo in the NIR (top) and visible wavelengths (bottom) for a vegetated planet (gray) and a planet with no vegetation (black) between phase angles 0.5° and 3.5° and 44° and 47° at different levels of planetary cloudiness (50–70%). Error bars (standard deviation) show differences between 12 simulations representing average global cloud cover for each month of the year.
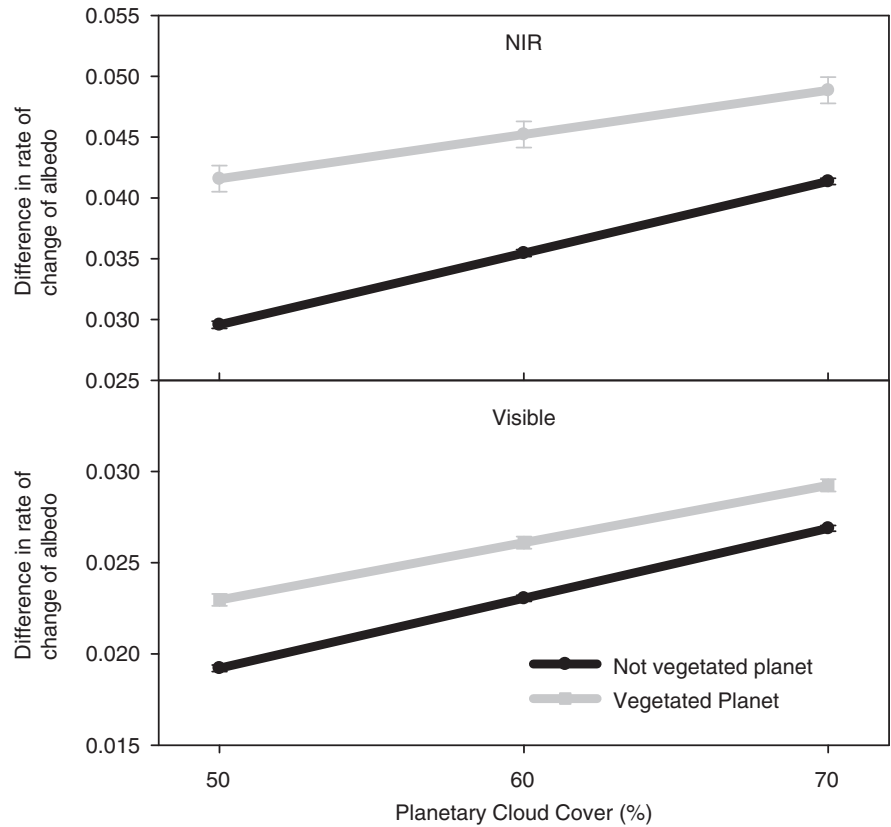
with abundant water or a planet covered with microbial life. Assuming that most physical processes that affect cloud formation on extrasolar planets habitable to multicellular life are similar to those on Earth, variations in cloud cover or height should not change enough between dichotomy and full illumination to mimic a vegetation hot spot. However, we cannot just subtract the albedo at phase angle 0.5° from albedo at phase angle 44° to determine whether there is vegetated life on a planet because this number will vary depending on total percentage cloud cover. If the rotation period can be determined with accuracy on an exoplanet, deviations from a periodic signal can be used to infer the
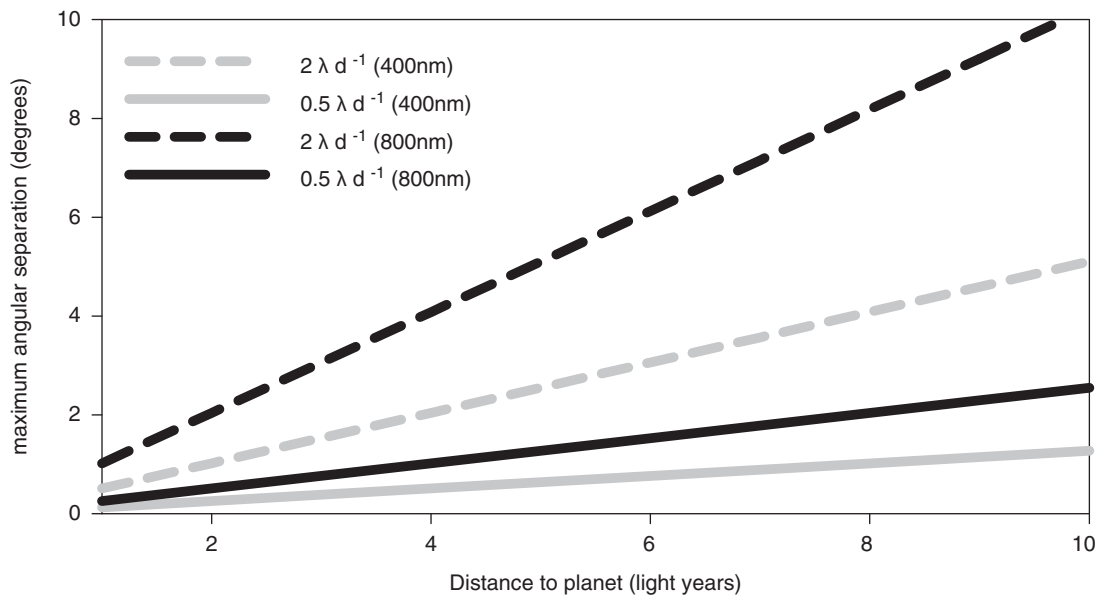

FIG. 7. The minimum distance an exoplanet can be resolved from its star (degrees) using two potential coronagraph designs, $2 \lambda\, d^{-1}$ (dashed lines) and $0.5 \lambda\, d^{-1}$ (solid lines), and two wavelengths, 400 nm (gray) and 800 nm (black), assuming an Earth-like orbit (1 AU).
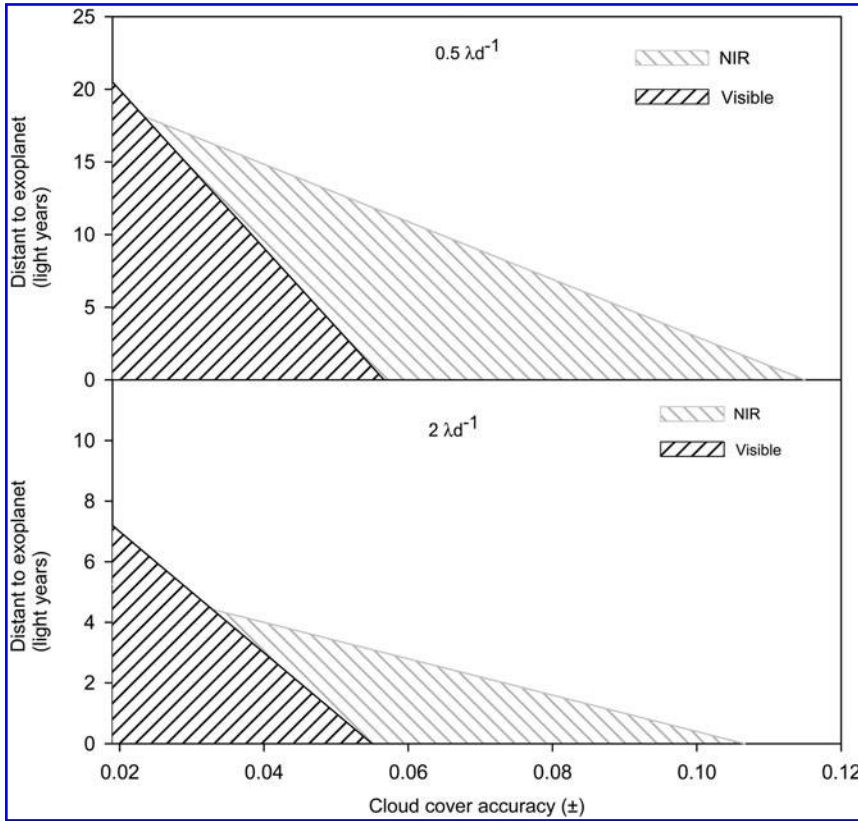
FIG. 8. The maximum distance (light-years) to exoplanet this method could potentially resolve multicellular life using different coronagraph designs, 0.5 λ d^{-1} (top) and 2 λ d^{-1} (bottom), and different wavelengths, visible (black) and NIR (gray). Cloud cover accuracy refers to what resolution planetary cloud cover needs to be resolved ($\pm$) to distinguish a planet with multicellular life from one without multicellular life.

presence of relatively short-lived structures such as clouds (Palle *et al.*, 2008).

Even if cloud cover cannot be determined with accuracy, we can exploit the differing rate of change of planetary albedo between vegetated and non-vegetated planets. This capitalizes on the fact that clouds and trees increase in brightness at distinctly different rates as a planet approaches full illumination: clouds exhibit forward scattering (Mishchenko *et al.*, 1996; Gatebe *et al.*, 2003), while trees exhibit backscattering (Bicheron and Leroy, 2000). This means that trees will increase in brightness as a planet approaches full illumination, as the shadows are hidden; but clouds will increase much less.

According to our simulations, we can detect multicellular life on an Earth-like planet by using the 2nd derivative of planetary albedo with respect to phase angle between phase angles $0.5°$ and $3.5°$ and $44°$ and $47°$. Planetary cloud cover can vary by ± 0.01 between the monthly maximum and the monthly minimum. However, this month-to-month change in cloud cover has only minor effects on the 2nd derivative with respect to phase angle of brightness as shown by the small error bars in Fig. 6. This additional constraining observation of BRDF may be sufficient to discriminate multicellular life from single-celluled life on extrasolar planets. In addition, using the rate of change of albedo will eliminate the need to estimate ground albedo accurately, which is not likely to be known with accuracy.

A dry lifeless planet similar to the Moon exhibits a strong hot spot due to shadows from craters and very dry fine soils that cause coherent backscatter. Coherent backscatter can occur on very dry soils where particles have a diameter that is similar to the wavelength of the photon used to view them.

This hot spot occurs because portions of wave fronts that are multiply scattered within a non-uniform, wavelength-sized medium combine after following the same path, but in opposite directions (Hapke *et al.*, 1993). In this study, we assumed that there would be no coherent backscatter on wet planets capable of sustaining multicellular life when the planets are viewed with wavelengths of 800 nm or less. On Earth, dry areas, such as deserts, generally have particle sizes of 0.05 to 2 mm (Tarbuck *et al.*, 2008), which are too big to exhibit coherent backscatter at 800 nm wavelengths. Desert areas can also exhibit hot spot features through geometric shadow processes, but the amplitude of the change in reflectance between the hot spot and dark spot is small, as exemplified by the BRDF of a barren region of Libya (Bicheron and Leroy, 2000). Wet areas would not exhibit coherent backscatter because extremely dry conditions (such as those present on the Moon) are necessary (Hapke *et al.*, 1996).

Mountains, asteroid craters, or other shadow-casting geological features can potentially confound the attribution of BRDF to multicellular life. However, most geological features such as asteroid craters or steep mountains ($>45°$ slope) will be eroded by abundant liquid water, an oxygen atmosphere, and an active geology, all of which are likely to be present on any planet capble of sustaining multicellular life (Kasting and Catling, 2003). A lifeless planet with a similar climate to Earth will be topologically very similar to Earth, although most sediment will be less weathered (Dietrich and Perron, 2006). Therefore, we can assume that, in terms of slope, Earth is typical of wet terrestrial planets with <1% of the surface with a slope greater than $45°$ (Hall *et al.*, 2005). We removed observations made at phase angles larger than $45°$ to ensure that any confounding effects of

steep terrain are small. On other planets, as on Earth, there may be unique topological features, like the hoodoo formations in Bryce Canyon or the limestone formations in Guilin, China, that exhibit backscattering anisotropic effects. However, hoodoo structures will likely be uncommon (<1% for the surface), as they need a rare combination of basalt and tuff to form and will eventually succumb to erosion. Limestone is of mainly marine biogeochemical origin, from shells and corals (Tarbuck *et al.,* 2008), and is likely to be less abundant on a lifeless planet.

The ocean and clouds dominate the albedo of Earth and will play an important role in determining the albedo of any exoplanet with abundant liquid water. The ocean and clouds forward scatter light, while trees backscatter light. Most of the change in reflectance from anistopic effects for clouds (Mishchenko *et al.,* 1996) and the ocean (Jin *et al.,* 2004) is from phase angles >45°. By removing phase angles >45°, we can also remove confounding anistropic effects of clouds and oceans. Typical ocean glint is 0.2 in the specular direction (Bréon and Henriot, 2006). However, reflectance in the specular direction will only rarely replicate the effect of a vegetation hot spot and, therefore, will not impact our results.

Is this method as useful for detecting life on exoplanets as using the red edge? The change in reflectance between the hot spot and the dark spot of a forest can be as large as the change in reflectance between the visible and NIR of a forest. For instance, the reflectance of a tropical broadleaf evergreen forest can increase by 0.3 between the hot spot and the dark spot (Bicheron and Leroy, 2000). This is similar to the increase in surface reflectance of a forest from 0.03 at 400 nm to 0.27 at 800 nm (Tinetti *et al.,* 2006a). Previous simulations have shown the difficulty of resolving the red edge if an exoplanet is resolved to a single pixel (Tinetti *et al.,* 2006b). Our simulations suggest that, by using advanced coronagraph designs and accurately resolving planetary cloud cover, a BRDF signal of life could be as large as a red-edge signal for nearby stellar systems.

To determine the optimal wavelength for this technique, it is first necessary to know how well cloud cover on an exoplanet can be resolved (Palle *et al.,* 2008). We determine that, if planetary cloud cover can be resolved to better $\sim \pm 0.03$, then 400 nm wavelength is optimal; otherwise, 800 nm wavelength is optimal (Fig. 8). In theory, a broadband albedo would work as well as a narrowband albedo. It has been hypothesized that planets with dimmer stars may have a red edge at higher wavelengths (Wolstencroft and Raven, 2002). In such a case, additional calculations will be necessary to determine optimal wavelengths.

How well this method could work is dependent on coronagraph design (Guyon *et al.,* 2006) and how well cloud cover can be resolved (Palle *et al.,* 2008) (Fig. 8). There are ~ 50 stellar systems within 5 parsecs of Earth. If cloud cover on exoplanets can be resolved to better than ± 0.03, then we estimate that this method may be effective on some of these stellar systems with currently possible coronagraph designs ($2 \lambda \, d^{-1}$) and on all of these stellar systems if future coronagraphs can be designed to resolve exoplanets to within $0.5 \lambda \, d^{-1}$ of their star (Table 2). Recently, an exoplanet 129 light-years away was resolved at $2 \lambda \, d^{-1}$ with a small (1.5 m) ground-based telescope (Serabyn *et al.,* 2010). This demonstrates the potential of this method to be used with ground-based telescopes capable of much larger lens

Table 2. The Distance to an Exoplanet That Multicellular Life May Be Detected, Assuming a 12-Meter Diameter Aperture Telescope and the Optimal Wavelength (400 or 800 nm) Based on Cloud Resolution Accuracy ($\pm$) and Coronagraph Design

	± 0.1	± 0.05	± 0.03
$2 \lambda \, d^{-1}$	1 light-year	4 light-years	6 light-years
$0.5 \lambda \, d^{-1}$	3 light-years	14 light-years	18 light-years

diameters that could further expand the range of this technique.

We can envision a process where a terrestrial exoplanet's size, density, cloud cover, distance to star, and the star's irradiance are measured or estimated. Based on these data, a model can be developed with which to estimate how albedo would change between 0° and 45° phase angles, assuming a relatively smooth, eroded, planetary surface. These simulations can be compared to the actual rate of change of brightness observed. If the rate of change of brightness between 0.5° and 3° and 44° and 47° is greater than the modeled estimate, then this is evidence for multicellular life on the planet. False positives caused by instrument error or intermittent events such as volcanic activity or changing cloud cover could be determined by observing the planet during continuous rotation cycles. Multicellular life would continuously demonstrate the BRDF signal, while other causes would demonstrate it only intermittently.

5. Conclusions

We can articulate four archetypal scenarios of planetary life: a dry lifeless planet, a lifeless planet with abundant liquid water, a planet with abundant liquid water and microbial life, and a planet with abundant liquid water and multicellular life (Table 3). Ideally, a set of observational constraints can be made that can distinguish these characteristics for a candidate planet. A dry lifeless planet will likely exhibit a hot spot due to abundant craters and wavelength-sized dust (Hapke *et al.,* 1993), but it will not exhibit signs of clouds or atmospheric water vapor. A lifeless planet with abundant liquid water will likely not exhibit a hot spot but will exhibit signs of clouds and atmospheric water. A planet with abundant liquid water and single-celled life will exhibit clouds, water, potentially a red-edge signal, but no BRDF effect (Tinetti *et al.,* 2006b). A planet with abundant liquid water and abundant multicellular life will exhibit signs of clouds, water, red edge, and a BRDF effect. If anisotropic effects are taken into account, tree-like multicellular life may be distinguished from single-celluled life on an exoplanet.

Table 3. Four Scenarios of Planets with Distinct Spectra for Indicators of Life

	Habitable	Red edge	BRDF effect
Dry lifeless	No	No	Yes
Lifeless + water	Yes	No	No
Microbial + water	Yes	Maybe	No
Multicellular + water	Yes	Yes	Yes

Abbreviations

BRDF, bidirectional reflectance distribution function; NIR, near infrared; TPF, Terrestrial Planet Finder.

References

Bacour, C. and Bréon, F.M. (2005) Variability of biome reflectance directional signatures as seen by POLDER. *Remote Sensing of Environment* 98:80–95.

Beerling, D. (2007) *The Emerald Planet: How Plants Changed Earth's History,* Oxford University Press, New York.

Bicheron, P. and Leroy, M. (2000) Bidirectional reflectance distribution function signatures of major biomes observed from space. *J Geophys Res* 105:26669–26681.

Bréon, F.M. and Henriot, N. (2006) Spaceborne observations of ocean glint reflectance and modeling of wave slope distributions. *J Geophys Res* 111, doi:10.1029/2005JC003343.

Bréon, F.M., Vanderbilt, V., Leroy, M., Bicheron, P., Walthall, C.L., and Kalshoven, J.E. (1997) Evidence of hot spot directional signature from airborne POLDER measurements. *IEEE Trans Geosci Remote Sens* 35:479–484.

Bréon, F.M., Maignan, F., Leroy, M., and Grant, I. (2002) Analysis of hot spot directional signatures measured from space. *J Geophys Res* 107, doi:10.1029/2001JD001094.

Brown, J.H. and West, G.B., editors. (2000) *Scaling in Biology,* Oxford University Press, New York.

Cockell, C.S., Léger, A., Fridlund, M., Herbst, T.M., Kaltenegger, L., Absil, O., Beichman, C., Benz, W., Blanc, M., Brack, A., Chelli, A., Colangeli, L., Cottin, H., Coudé du Foresto, F., Danchi, W.C., Defrère, D., den Herder, J.-W., Eiroa, C., Greaves, J., Henning, T., Johnston, K.J., Jones, H., Labadie, L., Lammer, H., Launhardt, R., Lawson, P., Lay, O.P., LeDuigou, J.-M., Liseau, R., Malbet, F., Martin, S.R., Mawet, D., Mourard, D., Moutou, C., Mugnier, L.M., Ollivier, M., Paresce, F., Quirrenbach, A., Rabbia, Y.D., Raven, J.A., Rottgering, H.J.A., Rouan, D., Santos, N.C., Selsis, F., Serabyn, E., Shibai, H., Tamura, M., Thiébaut, E., Westall, F., and White G.J. (2009) Darwin—a mission to detect and search for life on extrasolar planets. *Astrobiology* 9:1–22.

Collins, W.D., Rash, P., Boville, B.A., Hack, J.J., McCaa, J.R., Williamson, D.L., and Briegleb, B.P. (2006) The formulation and atmospheric simulation of the Community Atmosphere Model version 3 (CAM3). *J Clim* 19:2144–2161.

Des Marais, D.J., Harwit, M.O., Jucks, K.W., Kasting, J.F., Douglas, N.C., Lunine, J.I., Schneider, J., Seager, S., Traub, W.A., and Woolf, N.J. (2002) Remote sensing of planetary properties and biosignatures on extrasolar terrestrial planets. *Astrobiology* 2:153–181.

Dietrich, W.E. and Perron, J.T. (2006) The search for a topographic signature of life. *Nature* 439:411–418.

Donoghue, M.J. (2005) Key innovations, convergence, and success: macroevolutionary lessons from plant phylogeny. *Paleobiology* 31:77–93.

Enquist, B.J., Brown, J.H., and West, G.B. (1998) Allometric scaling of plant energetics and population density. *Nature* 395:163–165.

Ford, E.B., Seager, S., and Turner, E.L. (2001) Characterization of extrasolar terrestrial planets from diurnal photometric variability. *Nature* 412:885–887.

Gatebe, C.K., King, M.D., Platnick, S., Arnold, G.T., Vermote, E.F., and Schmid, B. (2003) Airborne spectral measurements of surface-atmosphere anisotropy for several surfaces and ecosystems over southern Africa. *J Geophys Res* 108, doi:10.1029/2002JD002397.

Gay, J. and Rabbia, Y. (1996) An interferometric method for coronography. *Comptes Rendus De L Academie Des Sciences Serie II Fascicule B-Mecanique Physique Chimie Astronomie* 322:265–271.

Graham, L.E., Cook, M.E., and Busse, J.S. (2000) The origin of plants: body plan changes contributing to a major evolutionary radiation. *Proc Natl Acad Sci USA* 97:4535–4540.

Guyon, O., Pluzhnik, E.A., Galicher, R., Martinache, F., Ridgway, S.T., and Woodruff, R.A. (2005) Exoplanet imaging with a phase-induced amplitude apodization coronagraph. I. Principle. *Astrophys J* 622:744–758.

Guyon, O., Pluzhnik, E.A., Kuchner, M.J., Collins, B., and Ridgway, S.T. (2006) Theoretical limits on extrasolar terrestrial planet detection with coronagraphs. *Astrophys J Suppl Ser* 167:81–99.

Hall, O., Falorni, G., and Bras, R.L. (2005) Characterization and quantification of data voids in the shuttle radar iopography mission data. *IEEE Geoscience and Remote Sensing Letters* 2:177–181.

Hapke, B., DiMucci, D., Nelson, R., and Smythe, W. (1996) The cause of the hot spot in vegetation canopies and soils: shadow-hiding versus coherent backscatter. *Remote Sensing of Environment* 58:63–68.

Hapke, B.W., Nelson, R.M., and Smythe, W.D. (1993) The opposition effect of the Moon—the contribution of coherent backscatter. *Science* 260:509–511.

Horodyski, R.J. and Knauth, L.P. (1994) Life on land in the Precambrian. *Science* 263:494–498.

Jin, Z.H., Charlock, T.P., Smith, W.L., and Rutledge, K. (2004) A parameterization of ocean surface albedo. *Geophys Res Lett* 31, doi:10.1029/2004GL021180.

Kasting, J.F. and Catling, D. (2003) Evolution of a habitable planet. *Annu Rev Astron Astrophys* 41:429–463.

Kenny, R. and Knauth, L.P. (2001) Stable isotope variations in the Neoproterozoic Beck Spring Dolomite and Mesoproterozoic Mescal Limestone paleokarst: implications for life on land in the Precambrian. *Geol Soc Am Bull* 113:650–658.

Kiang, N.Y, Segura, A., Tinetti, G., Blankenship, R.E., Cohen, R., Siefert, J., Crisp, D., and Meadows, V.S. (2007a) Spectral signatures of photosynthesis. II. Coevolution with other stars and the atmosphere on extrasolar worlds. *Astrobiology* 7:252–274.

Kiang, N.Y., Segura, A., Tinetti, G., Blankenship, R.E., Cohen, R., Siefert, J., Crisp, D., and Meadows, V.S. (2007b) Spectral signatures of photosynthesis: coevolution with other stars and the atmosphere on extrasolar worlds. *Astrobiology* 7:486–487.

Lawson, P.R., Lay, O.L., Johnston, K.J., and Beichman, C.A. (2007) Terrestrial Planet Finder Interferometer Science Working Group report. JPL Publication 07-1, Jet Propulsion Laboratory, California Institute of Technology, Pasadena, CA.

Li, X.W. and Strahler, A.H. (1992) Geometric-optical bidirectional reflectance modeling of the discrete crown vegetation canopy—effect of crown shape and mutual shadowing. *IEEE Trans Geosci Remote Sens* 30:276–292.

Lucht, W., Schaaf, C.B., and Strahler, A.H. (2000) An algorithm for the retrieval of albedo from space using semiempirical BRDF models. *IEEE Trans Geosci Remote Sens* 38:977–998.

Maignan, F., Breon, F.M., and Lacaze, R. (2004) Bidirectional reflectance of Earth targets: evaluation of analytical models using a large set of spaceborne measurements with emphasis on the hot spot. *Remote Sensing of Environment* 90: 210–220.

Mishchenko, M.I., Rossow, W.B., Macke, A., and Lacis, A.A. (1996) Sensitivity of cirrus cloud albedo, bidirectional reflectance and optical thickness retrieval accuracy to ice particle shape. *J Geophys Res* 101:16973–16985.

Oleson, K.W. and Bonan, G.B. (2000) The effects of remotely sensed plant functional type and leaf area index on simulations of boreal forest surface fluxes by the NCAR land surface model. *Journal of Hydrometeorology* 1:431–446.

Palle, E., Ford, E.B., Seager, S., Montanes-Rodriguez, P., and Vazquez, M. (2008) Identifying the rotation rate and the presence of dynamic weather on extrasolar Earth-like planets from photometric observations. *Astrophys J* 676:1319–1329.

Palle, E., Osorio, M.R.Z., Barrena, R., Montanes-Rodriguez, P., and Martin, E.L. (2009) Earth's transmission spectrum from lunar eclipse observations. *Nature* 459:814–816.

Sagan, C., Thompson, W.R., Carlson, R., Gurnett, D., and Hord, C. (1993) A search for life on Earth from the Galileo spacecraft. *Nature* 365:715–721.

Schaepman-Strub, G., Schaepman, M.E., Painter, T.H., Dangel, S., and Martonchik, J.V. (2006) Reflectance quantities in optical remote sensing—definitions and case studies. *Remote Sensing of Environment* 103:27–42.

Seager, S., Turner, E.L., Schafer, J., and Ford, E.B. (2005) Vegetation's red edge: a possible spectroscopic biosignature of extraterrestrial plants. *Astrobiology* 5:372–390.

Serabyn, E., Mawet, D., and Burruss, R. (2010) An image of an exoplanet separated by two diffraction beamwidths from a star. *Nature* 464:1018–1020.

Tarbuck, E.J., Lutgens, F.K., and Tasa, D. (2008) *Earth, An Introduction to Physical Geology*, 8th ed., Prentice Hall, Upper Saddle River, NJ.

Tinetti, G., Meadows, V.S., Crisp, D., Fong, W., Velusamy, T., and Snively, H. (2005) Disk-averaged synthetic spectra of Mars. *Astrobiology* 5:461–482.

Tinetti, G., Meadows, V.S., Crisp, D., Fong, W., Fishbein, E., Turnbull, M., and Bibring, J. (2006a) Detectability of planetary characteristics in disk-averaged spectra. I: The Earth model. *Astrobiology* 6:34–47.

Tinetti, G., Meadows, V.S., Crisp, D., Fong, W., Fishbein, E., Turnbull, M., and Bibring, J. (2006b) Detectability of planetary characteristics in disk-averaged spectra II: synthetic spectra and light-curves of earth. *Astrobiology* 6:881–900.

Torrance, K.E. and Sparrow, E.M. (1967) Theory for off-specular reflection from roughened surfaces. *J Opt Soc Am* 57:1105–1114.

West, G.B., Brown, J.H., and Enquist, B.J. (1999) A general model for the structure and allometry of plant vascular systems. *Nature* 400:664–667.

West, G.B., Enquist, B.J., and Brown, J.H. (2009) A general quantitative theory of forest structure and dynamics. *Proc Natl Acad Sci USA* 106:7040–7045.

Wolf, A., Berry, J.A., and Asner, G.P. (2010) Allometry constrains sources of variability in multi-angle reflectance measurements. *Remote Sensing of Environment* 14:1205–1219.

Wolstencroft, R.D. and Raven, J.A. (2002) Photosynthesis: likelihood of occurrence and possibility of detection on Earth-like planets. *Icarus* 157:535–548.

Address correspondence to:
Christopher E. Doughty
Carnegie Institution
Department of Global Ecology
Stanford, CA 92697-3100

E-mail: Chris.doughty@ouce.ox.ac.uk